# **Epitaxially Crystallized Polyethylene Exhibiting Near-Equilibrium Melting Temperatures**

Yucheng Wang<sup>1</sup>, Kaichen Gu<sup>1</sup>, Jason X. Liu<sup>2</sup>, Anishkumar Soman<sup>3</sup>, Tingyi Gu<sup>3</sup>, Craig B. Arnold<sup>2,4</sup>, Richard A. Register<sup>1,4</sup>, Yueh-Lin Loo<sup>1</sup>, Rodney D. Priestley<sup>1,4\*</sup>

<sup>1</sup>Department of Chemical and Biological Engineering, Princeton University, Princeton, New Jersey 08544, United States

<sup>2</sup>Department of Mechanical and Aerospace Engineering, Princeton University, Princeton, New Jersey 08544, United States

<sup>3</sup>Department of Electrical and Computer Engineering, University of Delaware, Newark, Delaware 19711, United States

<sup>4</sup>Princeton Institute for the Science and Technology of Materials, Princeton University, Princeton, New Jersey 08544, United States

\*rpriestl@princeton.edu

### **Keywords**

Epitaxial polymer crystallization, graphene, matrix-assisted pulsed laser evaporation (MAPLE), melting

#### **Abstract**

The morphology and orientation of polymer crystals are important factors which determine the performance of thin-film, polymer-enabled technologies such as organic electronics and gas separation membranes. Here, we utilize polymer-substrate epitaxy to achieve a highly oriented crystalline morphology during thin-film processing. To accomplish this, we employ matrix-assisted pulsed laser evaporation (MAPLE), a slow physical vapor deposition process, to deposit linear polyethylene atop an epitaxial graphene substrate. Via MAPLE, we demonstrate the ability to achieve a film morphology comprised of well-aligned, edge-on crystalline lamellae. Furthermore, we show that MAPLE can be exploited to grow crystalline lamellae composed entirely of extended polymer chains which exhibit a near-equilibrium melting temperature. Our work demonstrates that MAPLE, as a bottom-up approach, can deposit polymer thin films with improved control over crystalline morphology.

### **Main Text**

Enforcing the crystallization of polymers into a desired thin-film morphology remains a major scientific challenge. 1-4 Yet, the morphology is a critical factor determining the performance of next-generation thin-film polymeric systems in which crystallite size, orientation, degree of crystallinity, and inter-crystalline structure strongly influence properties such as charge transport efficiency in organic electronics, 5-10 gas permeability in barrier coatings, 11,12 and mechanical properties in polymer nanocomposites. 13-15 One method to control the crystalline morphology of thin films atop substrates is to employ epitaxial growth, in which there is a geometric and energetically favorable match between polymer inter-chain distances and substrate interplanar spacings. 16-18 For example, thin films of polyethylene (PE) spun-cast atop graphene can exhibit well-ordered morphologies composed of epitaxial, edge-on lamellae instead of the typical disordered spherulitic structures observed atop substrates which exhibit no epitaxial lattice matching, such as silicon. 19 However, the rapid solidification of solution-processed PE films precludes the formation of fully-extended chain crystals in uniform films, as equilibrium conditions are not reached. 20,21

As an alternative to rapid solution processing, physical vapor deposition (PVD) presents a technique of slow thin film deposition. In conventional laser-based PVD, ultrathin films of atomic and molecular species can be deposited atop various substrates via laser ablation under high vacuum. However, traditional PVD results in chemical degradation when depositing organic materials with molecular weights greater than ~1000 g/mol.<sup>1,22</sup> Recently, a technique termed matrix-assisted pulsed laser evaporation (MAPLE) was developed to overcome this limitation by protecting the polymer chains with a sacrificial solvent that constitutes >95% wt. of the ablation target.<sup>23–25</sup> Deposition occurs via the coalescence of nanoscopic polymer globules created from the laser ablation plume. In contrast to solution processing, MAPLE offers greater control over film deposition by controlling key process parameters, such as target composition, deposition rate, and substrate temperature and chemistry.<sup>26,27</sup>

Here, we utilize the precise control afforded by MAPLE to deposit ultrathin layers of PE crystals which epitaxially crystallize atop graphene. By performing MAPLE deposition at elevated temperatures, we circumvent conventional issues associated with solution processing of polymer thin films, which is more difficult to control. We reveal a highly oriented crystalline structure exhibiting stacked, edge-on lamellae, strictly aligned parallel to the surface plane. Atomic force microscopy (AFM) measurements show that these lamellae are 27 nm in length, which compares

well to the fully-extended chain length for the PE employed in the study. We show that at the interface, PE adopts an orthorhombic structure. We perform in-situ grazing-incidence x-ray diffraction (GIXD) with thermal ramping to probe the melting temperature of deposited PE crystals. We show that, remarkably, MAPLE-deposited epitaxial PE crystals atop graphene exhibit a near-equilibrium melting temperature,  $T_m$ , of 140°C. Upon melt-recrystallization, the PE crystals retain their edge-on orientation and films show a minor increase of  $T_m$  relative to the bulk melting temperature of 127.8°C, demonstrating that the enhancement is unique to the slow deposition of the MAPLE method.

For MAPLE, we used a 0.2 mg/mL solution of linear polyethylene ( $M_n = 3000 \text{ g/mol}$ ,  $M_w/M_n$ = 1.10) dissolved in p-xylene and subsequently frozen in liquid nitrogen as the target. A pulsed UV laser with  $\lambda$  = 248 nm was used to ablate the target. We performed depositions atop both single-layered graphene and silicon wafers. Additional experimental details can be found in the Materials and Methods section. The ability of MAPLE-deposited epitaxial PE crystals to exhibit near-equilibrium melting temperatures is attributed to the mechanism of slow additive growth. Film growth by MAPLE deposition occurs via the sequential addition of polymer clusters which range from tens of nanometers to a few microns in diameter.<sup>24,28</sup> For a one-hour long deposition, we fabricated films of ~10 nm average thickness, as measured by AFM. This allowed us to probe the crystalline morphology near the epitaxial substrate interface. As polymer chains reached the substrate during deposition, the substrate temperature,  $T_{sub}$ , can effectively approximate the crystallization temperature,  $T_c$  (<  $T_m$ ), and impact both the driving force for crystallization and polymer chain mobility, thus dictating the resulting crystal structure. In our experiments, we maintained the substrate temperature at 100°C to favor the growth of extended-chain PE crystals. The high substrate temperature promotes the formation of fully-extended crystals by both increasing polymer chain mobility and reducing the driving force for chain attachment to the crystal surface.

**Figure 1** depicts the epitaxial alignment of polymer crystals enabled by MAPLE deposition. Roughly 10 nm thick films of PE were deposited atop graphene and silicon substrates under the same conditions: ~10 nm/h growth rate at  $T_{sub} = 100$ °C. **Figure 1b** depicts a representative AFM image of the film deposited atop silicon. The globular morphology resulting from MAPLE deposition is immediately apparent, with crystallized droplets decorating the substrate. Due to the lack of attractive interactions between PE and the silicon substrate, the polymer does not wet the substrate and crystallizes within the as-deposited globules with no

preferential orientation. In the AFM phase images, lamellae can be seen oriented approximately in the same direction within each isolated droplet, but with no global orientational order between different droplets. Alternatively, **Figure 1a** depicts a PE film deposited atop graphene, in which oriented crystallites were observed to align along angles separated by 120°, epitaxially matching the underlying graphene's three-fold symmetry. Due to the low interfacial tension between PE and graphene,<sup>29</sup> the MAPLE-deposited globules wet the graphene substrate. Crystalline domains of uniform height (~10 nm), which span several hundreds of nanometers laterally, were observed. Within these domains, crystalline lamellae were observed to be well-oriented along the epitaxial directions. Given these characteristics, we infer that there was no vertical discontinuity: the lamellae are single crystals which extend directly to the graphene surface.

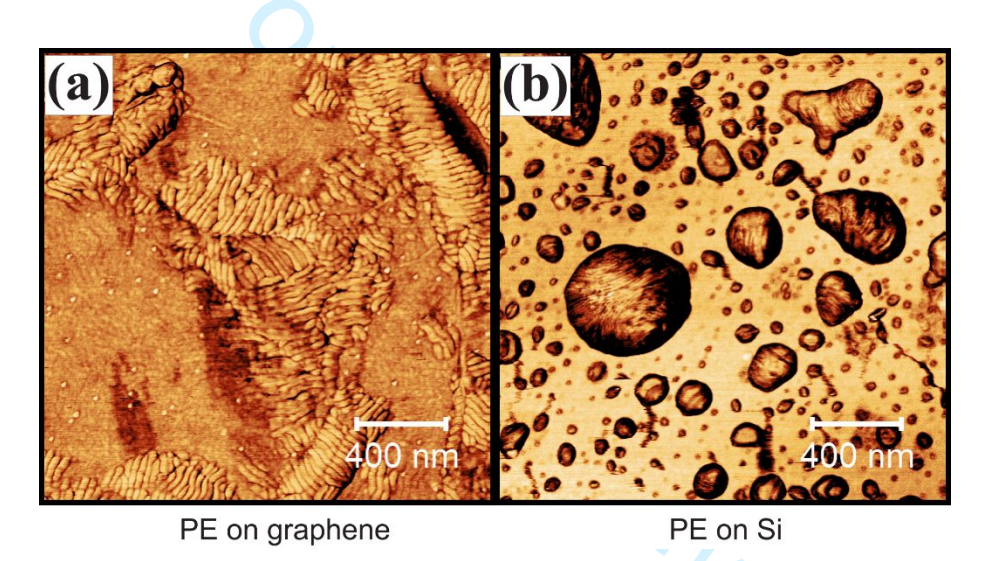


**Figure 1**: AFM phase images comparing the morphology of MAPLE-deposited PE crystals atop (a) graphene and (b) silicon. The substrate temperature was held constant at 100°C during both depositions. Both scale bars are 400 nm.

The highly oriented crystalline morphology was further revealed by grazing-incidence x-ray diffraction (GIXD) measurements. At room temperature, we collected a 2D diffraction pattern for MAPLE-deposited PE atop graphene, as shown in **Figure 2a**. The narrow azimuthal distribution of the crystal reflections indicates that the polymer chains were well-aligned, consistent with AFM observations. Furthermore, the diffraction pattern matched that of orthorhombic PE,<sup>30</sup> following the epitaxial relationship:  $(0001) < 2\overline{11}0 >_{graphene} // (110) < 001 >_{orthorhombic PE}$  at the PE-graphene interface upon MAPLE deposition.<sup>31</sup> In **Figure 2b**, we

demonstrate this relationship, in which the PE crystal is bisected along (110) to interact with the basal plane of graphene. It has been previously reported that for solution crystallized ultrathin films of PE (h < 20 nm,  $T_c \sim 100^{\circ}$ C), the metastable monoclinic crystal form preferentially existed at the graphene surface.<sup>32</sup> The lattice mismatch between PE and graphene is -5.0% and +4.3% for the monoclinic and orthorhombic forms, respectively. Thus, it was postulated that the expansion of the PE crystals to epitaxially match the monoclinic form was more energetically favorable than compression to match the orthorhombic form during rapid crystallization. In contrast, we observed the more thermodynamically stable polymorph, orthorhombic PE, for MAPLE deposited films. We hypothesize that the condition of slow additive film growth (~10 nm/h) and the simultaneous thermal annealing at  $T_{sub}$  = 100°C directly resulted in the equilibrium orthorhombic form.<sup>33,34</sup>

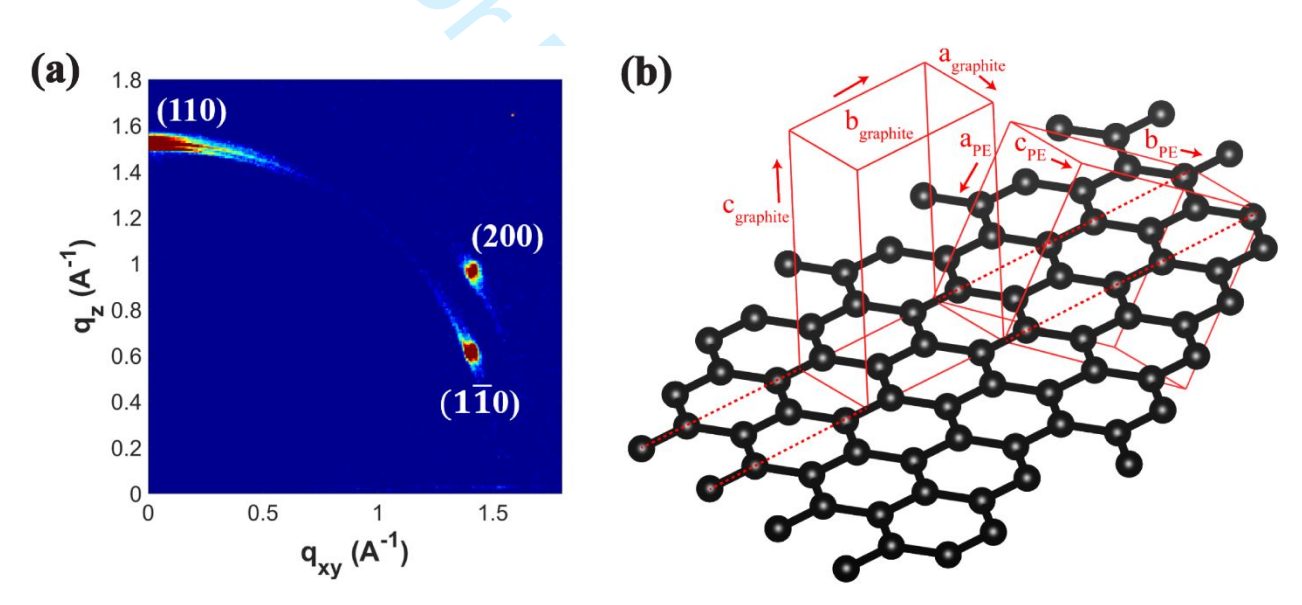


**Figure 2**: (a) Indexed GIXD pattern of MAPLE-deposited PE crystals atop the graphene surface; the scattering pattern was collected at room temperature. The GIXD pattern revealed the orthorhombic form of PE. The (110) crystal reflection is parallel to the surface plane, indicating the formation of edge-on lamellae. (b) A schematic depicting the relative orientation of the graphite and PE unit cells. The epitaxial relationship between the a-axis of graphite (graphene) and the c-axis of PE is denoted by the red dotted line.

When the deposited PE crystallizes, the extent of chain folding is indicative of the conditions under which crystallization occurred. The Lauritzen-Hoffmann relationship predicts the dependence of lamellar thickness on crystallization temperature, in which a higher crystallization

temperature yields thicker lamellae. However, PE in our MAPLE-deposited films exhibit preferential interactions with the substrate, which has strongly influenced the lamellar thickness. Remarkably, when deposited epitaxially atop graphene, the thickness of each PE crystalline lamella was measured by AFM to be ~27 nm, which equals the extended, single-chain length of our PE. In contrast, at the same substrate temperature and deposition conditions, the lamellar thickness of crystallites grown on silicon is substantially smaller, composed of once-folded polymer chains with 14 nm thickness on average<sup>35</sup>. The attainment of the fully-extended chain morphology can be attributed to a combination of the high substrate temperature during deposition and the epitaxial relationship. At a sufficiently high temperature of 100°C (the bulk crystallization temperature is ~114°C), the energetically favorable polymer-substrate epitaxy counteracts the crystallization driving force which forms folded-chain polymer crystals. However, when we performed MAPLE depositions at a much greater undercooling, the highly oriented, epitaxial edge-on lamellae were no longer observed by AFM and GIXD (see Supporting Figure S6); rather, smaller lamellae and a globular morphology are observed.

To characterize the increase in melting temperature induced by the epitaxial crystallization, we measured the melting and crystallization temperatures by in-situ GIXD measurements. This method is preferred due to the small total polymer mass of the thin films. We began by heating the as-deposited MAPLE films from room temperature to 150°C at 5°C/min. We considered  $T_{m,end}$  as the temperature at which the reflections associated with the orthorhombic PE crystals vanished from the diffraction pattern. In this case, we integrated the intensity azimuthally at  $q_{xy} \sim 1.5 \text{ Å}^{-1}$ , which corresponds to the combined (110) and (1 $\bar{1}$ 0) crystal reflections. Following complete melting at 150°C, we recrystallized PE by cooling at 5°C/min.  $T_{c,onset}$  was characterized as the temperature at which the PE reflections re-emerged. With an identical thermal cycling protocol (Figure S3), we compared the difference in  $T_m$  between MAPLE and non-MAPLE crystals, both grown epitaxially atop graphene.

We observed a significantly higher  $T_m$  for MAPLE-deposited PE films atop graphene relative to the bulk melting temperature ( $T_{m,bulk}$  = 127.8°C). **Figure 3a** shows the results from insitu GIXD experiments. Upon crystal melting, the integrated intensity from crystal reflections reduced with increasing temperature. We observed a sharp decrease in intensity at 138°C, with a further reduction until the complete disappearance of crystal reflections at  $T_{m,end} \sim 140$ °C, as shown in **Figure 3b**. Notably, the value is close to the estimated equilibrium melting temperature

of PE of 141°C.<sup>20,36,37</sup> We note that the increase in integrated intensity after the melt transition, beyond 145°C, is attributed to the volume expansion of the sample upon heating.

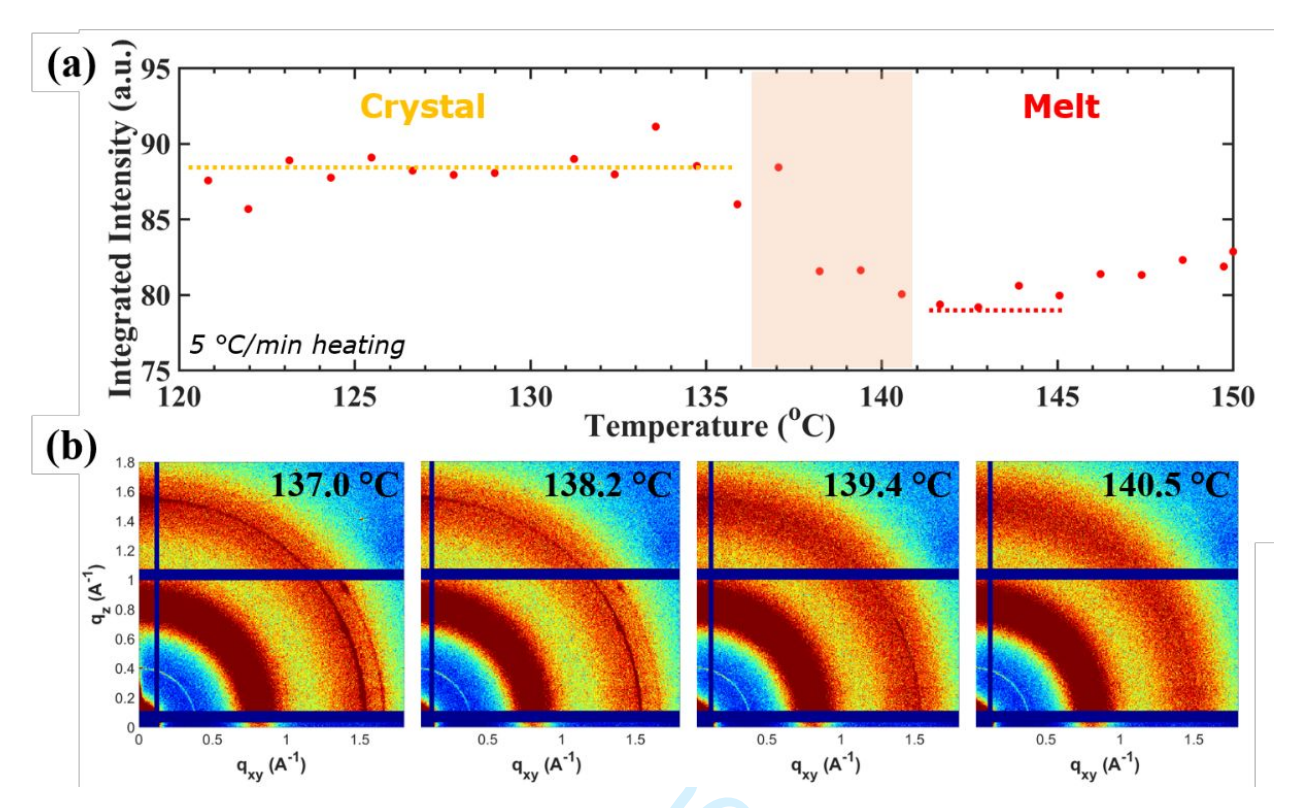


**Figure 3**: GIXD results characterizing  $T_m$  of MAPLE-deposited PE atop graphene. The substrate temperature during the original MAPLE deposition was  $100^{\circ}$ C. (a) Plot showing integrated intensity from PE crystal reflections of (110) and  $(1\overline{1}0)$  as a function of temperature. The heating rate was  $5^{\circ}$ C/min. (b) GIXD patterns at various temperatures in the vicinity of the melt transition.

Upon subsequent cooling, recrystallization occurred at  $T_{c,onset} \sim 124$  °C. This is indicated by the re-emergence of PE crystal reflections (Figure S4). The recrystallization temperature is greater than that of bulk recrystallization, where  $T_{c,peak} = 114.3$  °C was measured by differential scanning calorimetry. This increased recrystallization temperature on the epitaxial substrate agrees with observations for composite PE/graphene and PE/reduced graphene oxide nanosheets, where the epitaxial interface facilitates the nucleation of PE. 19,31,39 After being recrystallized at 5 °C/min, we once again melted the PE film atop graphene. In this case, however,  $T_{m,end} \sim 131$  °C, as shown in **Figure 4**. This melting temperature is closer to the bulk melting temperature,  $T_{m,bulk} = 127.8$  °C, and is substantially lower than that of as-MAPLE-deposited PE films atop graphene.

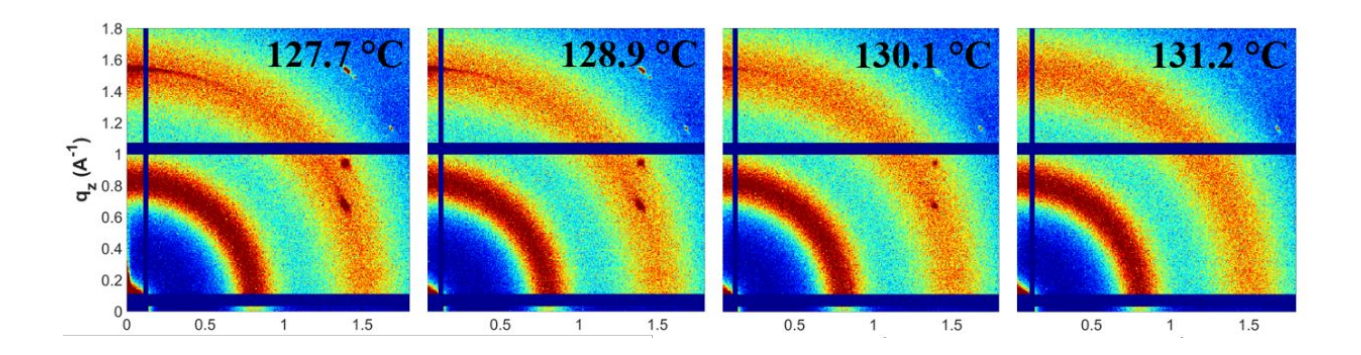


**Figure 4**: GIXD results measuring  $T_m$  of PE atop graphene recrystallized from the melt at 5°C/min. The crystallization temperature on the previous cooling step is  $T_{c,onset}$  = 124°C.

That MAPLE can yield a higher  $T_m$  than melt-recrystallized PE for an ultrathin layer atop an epitaxial substrate is attributed to the slow additive growth mechanism. In melt recrystallization, the crystallizing material is fully present during the phase transformation. On the other hand, film growth during MAPLE occurs via the separate addition of nanometer to micrometer-sized polymer chain clusters. The slow additive growth rate of 0.003 nm/s coupled with the graphene surface temperature of 100°C allows for ample rearrangement of PE chains before attachment to the crystal surface. Over the course of a 1-hour long deposition, these effects cooperate to effectively thermally anneal the crystals, allowing chains to undergo structural reorganization and further perfect the crystal structure by allowing most or all chains to achieve the fully-extended structure with no partial folding or re-entry at the fold surface. This increased crystal perfection reduces the fold surface free energy in the Gibbs-Thomson equation, thus yielding the further 10°C increase in the melting temperature over melt-recrystallized PE.

These results thus demonstrate how MAPLE is a viable processing technique that allows for the growth of ultrathin layers of polymer crystals atop epitaxial substrates. By depositing at sufficiently high substrate temperatures, the crystallization rate can be sufficiently slowed down to allow for substantial chain motion within each polymer cluster during crystallization. This, coupled with the slow growth rate achieved by MAPLE deposition, promotes the formation of highly oriented, epitaxial crystal structures. These effects conspire to minimize chain folding and allow for the direct growth of fully-extended chain crystals, avoiding the need for post-processing steps such as prolonged thermal annealing.<sup>20,21,40</sup> These structures exhibit near-equilibrium melting temperatures of ca. 140°C, and are unique to slow-growth addition via MAPLE. The capability of MAPLE deposition to grow near-equilibrium epitaxial structures may be utilized to

deposit highly oriented crystals for fundamental studies on polymer crystallization and applications.

#### **Materials and Methods**

The polymer used in this study was linear PE, POLYWAX® 3000 ( $M_n$  = 3000 g/mol,  $M_w/M_n$  = 1.10, with no detectable branching<sup>27</sup>), generously provided by Petrolite Corporation (Tulsa, OK). We prepared single layers of graphene ( $h \sim 0.25$  nm) by chemical vapor deposition atop a copper substrate, followed by copper etching and transferring to SiO<sub>2</sub>/Si substrates.

For MAPLE deposition, PE was fully dissolved in heated p-xylene at ~115°C with an overall concentration of 0.2 mg/ml. About 8 ml of the clear solution was then transferred to an aluminum target cup and rapidly frozen in a liquid nitrogen bath prior to insertion into a vacuum chamber. The substrates, i.e., graphene and silicon, were attached to a substrate holder with an electric heater, which was placed inside the chamber at a distance of ~6 cm away from the target cup. The chamber pressure was maintained at ~10-4 Torr throughout MAPLE deposition. Laser ablation was performed with a KrF laser (LightMachinery PulsedMaster 844,  $\lambda$  = 248 nm, pulse duration = 20 ns). The laser was operated at a fluence of 0.1 J/cm² and a repetition rate of 5 Hz. During MAPLE deposition, the target cup was kept frozen by circulating liquid-nitrogen-cooled nitrogen gas, and the substrate temperature was held constant by a PID controller. The deposition lasted 1 hour.

The Raman measurements were performed using a DXR Micro-Raman Spectroscope (Thermo Scientific) to measure the Stokes energy shift. The excitation was performed by a green laser ( $\lambda$  = 532 nm). The spot size was 700 nm for collecting the Raman spectra. To ensure a non-destructive measurement, a low power of 0.1 mW and a short laser exposure of 10 seconds were used. For room-temperature AFM measurements, a tapping mode AFM (Bruker Dimension ICON3) was employed. The AFM image processing and analysis were done using Gwyddion.

GIWAXS measurements were performed at the Complex Materials Scattering (CMS) beamline of the National Synchrotron Light Source II (NSLS-II), Brookhaven National Laboratory. The X-ray beam with an energy of 13.5 keV shone upon the samples between the critical angles of the organic film and the substrate. An incident angle of 0.1° was used for the ex-situ measurements and 0.12° for the in-situ measurements with respect to the substrate. A custom-made Pilatus-800K detector was placed 257 mm from the sample center to capture GIWAXS

images with an exposure time of 30 s and 10 s for the ex-situ and in-situ measurements, respectively. A Linkam stage (HFSX 350) was used to control the temperature of the samples during measurements. All GIWAXS images have been background subtracted.

# Acknowledgements

We acknowledge financial support from the National Science Foundation (NSF) Materials Research Science and Engineering Center Program through the Princeton Center for Complex Materials (DMR-1420541 and 2011750). K.G. and Y.-L.L. acknowledge the support of ExxonMobil through its membership in Princeton E-ffiliates Partnership of the Andlinger Center for Energy and the Environment. A. S. and T. G. are partially supported by AFOSR (FA9550-18-1-0300). We appreciate help from Dr. R. Li and Dr. E. Tsai on the x-ray scattering measurements. This research used the Center for Functional Nanomaterials (CFN) and the Complex Materials Scattering (CMS) beamline of the National Synchrotron Light Source II (NSLS-II), which both are U.S. DOE Office of Science Facilities, at Brookhaven National Laboratory under Contract No. DE-SC0012704.

### **Supporting Information Available**

The Supporting Information includes a micro-Raman spectrum of single-layered graphene, AFM height image and zoomed-in Micro-Raman spectrum to confirm the single-layer thickness of graphene, AFM height image of MAPLE-deposited PE atop graphene, thermal cycling protocol for in-situ GIXD measurements,  $T_c$  for PE melt-recrystallization atop graphene, and the morphology of MAPLE-deposited PE atop graphene prepared at a lower  $T_{sub}$  = 25°C.

#### References

- Lotz, B., Miyoshi, T. & Cheng, S. Z. D. 50th Anniversary Perspective: Polymer Crystals and Crystallization: Personal Journeys in a Challenging Research Field. *Macromolecules* 50, 5995–6025 (2017).
- 2. Son, H. J., Carsten, B., Jung, I. H. & Yu, L. Overcoming Efficiency Challenges in Organic Solar Cells: Rational Development of Conjugated Polymers. *Energy Environ. Sci.* **5**, 8158–8170 (2012).
- 3. Wang, G., Melkonyan, F. S., Facchetti, A. & Marks, T. J. All-Polymer Solar Cells: Recent Progress, Challenges, and Prospects Angewandte. *Angew. Chemie* 4129–4142 (2019) doi:10.1002/anie.201808976.
- 4. Wang, Y., Jeong, H., Chowdhury, M., Arnold, C. B. & Priestley, R. D. Exploiting physical vapor deposition for morphological control in semi-crystalline polymer films. *Polym. Cryst.* **1**, e10021 (2018).
- 5. Gu, K., Onorato, J. W., Luscombe, C. K. & Loo, Y.-L. The Role of Tie Chains on the Mechano-Electrical Properties of Semiconducting Polymer Films. *Adv. Electron. Mater.* **6**, 1901070 (2020).
- 6. Sirringhaus, H. 25th Anniversary Article: Organic Field-Effect Transistors: The Path Beyond Amorphous Silicon. *Adv. Mater.* **26**, 1319–1335 (2014).
- 7. Noriega, R. *et al.* A General Relationship Between Disorder, Aggregation and Charge Transport in Conjugated Polymers. *Nat. Mater.* **12**, 1038–1044 (2013).
- 8. Tumbleston, J. R. *et al.* The Influence of Molecular Orientation on Organic Bulk Heterojunction Solar Cells. *Nat. Photonics* **8**, 385–392 (2014).
- 9. Liu, Y. *et al.* Aggregation and Morphology Control Enables Multiple Cases of High-Efficiency Polymer Solar Cells. *Nat. Commun.* **5**, 1–8 (2014).
- 10. Liu, F., Gu, Y., Jung, J. W., Jo, W. H. & Russell, T. P. On the morphology of polymer-based photovoltaics. *J. Polym. Sci. Part B Polym. Phys.* **50**, 1018–1044 (2012).
- 11. Wang, H. *et al.* Confined Crystallization of Polyethylene Oxide in Nanolayer Assemblies. *Science* (80-.). **323**, 757–760 (2020).
- 12. Hiltner, A., Liu, R. Y. F., Hu, Y. S. & Baer, E. Oxygen Transport as a Solid-State Structure Probe for Polymeric Materials: A Review. *J. Polym. Sci. Part B Polym. Phys.* **43**, 1047–1063 (2005).
- 13. Jimenez, A. M. *et al.* Effects of Hairy Nanoparticles on Polymer Crystallization Kinetics. *Macromolecules* **52**, 9186–9198 (2019).
- 14. Wen, X. et al. Direct Relationship between Dispersion and Crystallization Behavior in Poly(ethylene oxide)/Poly(ethylene glycol)- g -Silica Nanocomposites . *Macromolecules* (2021) doi:10.1021/acs.macromol.0c02259.
- 15. Jimenez, A. M., Altorbaq, A. S., Muller, A. J. & Kumar, S. K. Polymer crystallization under confinement by well-dispersed nanoparticles. *Macromolecules* **53**, 10256–10266 (2020).
- 16. Mauritz, K. A., Baer, E. & Hopfinger, A. J. Epitaxial Crystallization of Macromolecules. *J Polym Sci Macromol Rev* **13**, 1–61 (1978).
- 17. Wellinghoff, S., Rybnikar, F. & Baer, E. Epitaxial Crystallization Of Polyethylene. *J. Macromol. Sci. Part B* **10**, 1–39 (1974).
- 18. Zhou, H., Jiang, S. & Yan, S. Epitaxial crystallization of poly(3-hexylthiophene) on a highly oriented polyethylene thin film from solution. *J. Phys. Chem. B* **115**, 13449–13454 (2011).
- 19. Löhmann, A.-K., Henze, T. & Thurn-Albrecht, T. Direct observation of prefreezing at the interface melt–solid in polymer crystallization. *Proc. Natl. Acad. Sci.* **111**, 17368–17372 (2014).
- 20. Hocquet, S. *et al.* Morphology and Melting of Truncated Single Crystals of Linear Polyethylene. *Macromolecules* **36**, 8376–8384 (2003).
- 21. Organ, S. J., Hobbs, J. K. & Miles, M. J. Reorganization and Melting of Polyethylene Single Crystals: Complementary TEM, DSC, and Real-Time AFM Studies. *Macromolecules* **37**,

- 4562-4572 (2004).
- 22. Wittmann, J. C. & Lotz, B. Polymer decoration: The orientation of polymer folds as revealed by the crystallization of polymer vapors. *J. Polym. Sci. Polym. Phys. Ed.* **23**, 205–226 (1985).
- 23. Andrew McGill, R. *et al.* Performance optimization of surface acoustic wave chemical sensors. *IEEE Trans. Ultrason. Ferroelectr. Freq. Control* **45**, 1370–1380 (1998).
- 24. Shepard, K. B. & Priestley, R. D. MAPLE deposition of macromolecules. *Macromol. Chem. Phys.* **214**, 862–872 (2013).
- Caricato, A. P., Ge, W. & Stiff-Roberts, A. D. UV- and RIR-MAPLE: Fundamentals and Applications. in *Advances in the Application of Lasers in Materials Science* (ed. Ossi, P. M.) 275–308 (Springer International Publishing, 2018). doi:10.1007/978-3-319-96845-2 10.
- 26. Wang, Y. et al. Tunable Properties of MAPLE-Deposited Thin Films in the Presence of Suppressed Segmental Dynamics. ACS Macro Lett. 1115–1121 (2019) doi:10.1021/acsmacrolett.9b00406.
- 27. Li, A., Dong, B. X. & Green, P. F. Influence of morphological disorder on in-and out-of-plane charge transport in conjugated polymer films-Erratum. *MRS Commun.* **5**, 646 (2015).
- 28. Shepard, K. B., Arnold, C. B. & Priestley, R. D. Origins of nanostructure in amorphous polymer coatings via matrix assisted pulsed laser evaporation. *Appl. Phys. Lett.* **103**, 3–6 (2013).
- 29. Tu, C., Nagata, K. & Yan, S. Influence of melt-mixing processing sequence on electrical conductivity of polyethylene/polypropylene blends filled with graphene. *Polym. Bull.* **74**, 1237–1252 (2017).
- 30. Bruno, J. A. O., Allan, N. L., Barron, T. H. K. & Turner, A. D. Thermal expansion of polymers: Mechanisms in orthorhombic polyethylene. *Phys. Rev. B* **58**, 8416–8427 (1998).
- 31. Cheng, S., Chen, X., Hsuan, Y. G. & Li, C. Y. Reduced graphene oxide-induced polyethylene crystallization in solution and nanocomposites. *Macromolecules* **45**, 993–1000 (2012).
- 32. Takenaka, Y. *et al.* Interface structure of epitaxial polyethylene crystal grown on HOPG and MoS2 substrates. *Macromolecules* **37**, 9667–9669 (2004).
- 33. Takahashi, Y. & Ishida, T. Monoclinic-to-orthorhombic Transformation in Polyethylene. *J. Polym. Sci. Part B Polym. Phys.* **26**, 2267–2277 (1988).
- 34. Olsson, P. A. T. *et al.* Ab initio investigation of monoclinic phase stability and martensitic transformation in crystalline polyethylene. *Phys. Rev. Mater.* **2**, 75602 (2018).
- 35. Jeong, H. *et al.* Tuning Morphology and Melting Temperature in Polyethylene Films by MAPLE. *Macromolecules* **51**, 512–519 (2018).
- 36. Harrison, I. R. Polyethylene single crystals: Melting and morphology. *J. Polym. Sci. Polym. Phys. Ed.* **11**, 991–1003 (1973).
- 37. Toda, A., Taguchi, K., Nozaki, K. & Konishi, M. Melting behaviors of polyethylene crystals: An application of fast-scan DSC. *Polymer (Guildf)*. **55**, 3186–3194 (2014).
- 38. Ueda, M. & Register, R. A. Crystallization-induced phase separation in mixtures of model linear and short-chain branched polyethylenes. *J. Macromol. Sci. Part B Phys.* **35**, 23–36 (1996).
- 39. Yao, G. *et al.* The influence of epitaxial crystallization on the mechanical properties of a high density polyethylene/reduced graphene oxide nanocomposite injection bar. *RSC Adv.* **7**, 21918–21925 (2017).
- 40. Asakawa, H., Nishida, K., Kanaya, T. & Tosaka, M. Giant single crystal of isotactic polypropylene showing near-equilibrium melting temperature. *Polym. J.* **45**, 287–292 (2012).

# **Supporting Information**

## **Epitaxially Crystallized Polyethylene Exhibiting Near-Equilibrium Melting Temperature**

Yucheng Wang<sup>1</sup>, Kaichen Gu<sup>1</sup>, Jason X. Liu<sup>2</sup>, Anishkumar Soman<sup>3</sup>, Tingyi Gu<sup>3</sup>, Richard A. Register<sup>1,4</sup>, Craig B. Arnold<sup>2,4</sup>, Yueh-Lin Loo<sup>1</sup>, Rodney D. Priestley<sup>1,4\*</sup>

<sup>1</sup>Department of Chemical and Biological Engineering, P[rinceton University, Princeton, New Jersey 08544, United States

<sup>2</sup>Department of Mechanical and Aerospace Engineering, Princeton University, Princeton, New Jersey 08544, United States

<sup>3</sup>Department of Electrical and Computer Engineering, University of Delaware, Newark, Delaware 19711, United States

<sup>4</sup>Princeton Institute for the Science and Technology of Materials, Princeton University, Princeton, New Jersey 08544, United States

<sup>\*</sup> rpriestl@princeton.edu

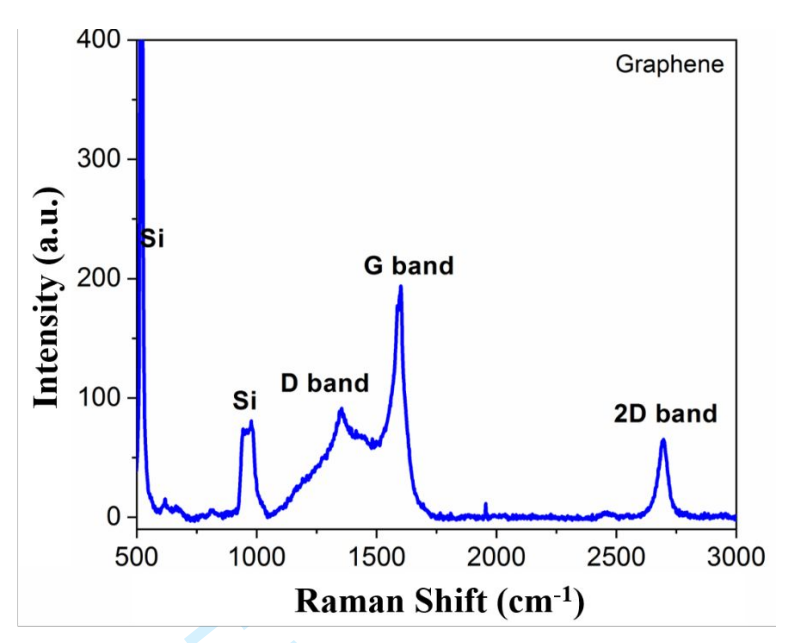


**Figure S1.** Micro-Raman spectrum of the graphene layer supported on SiO<sub>2</sub>/Si substrate. The characteristic bands of graphene are labeled as D, G, and 2D. The spectrum indicates that the supported graphene is of a single-layer thickness.

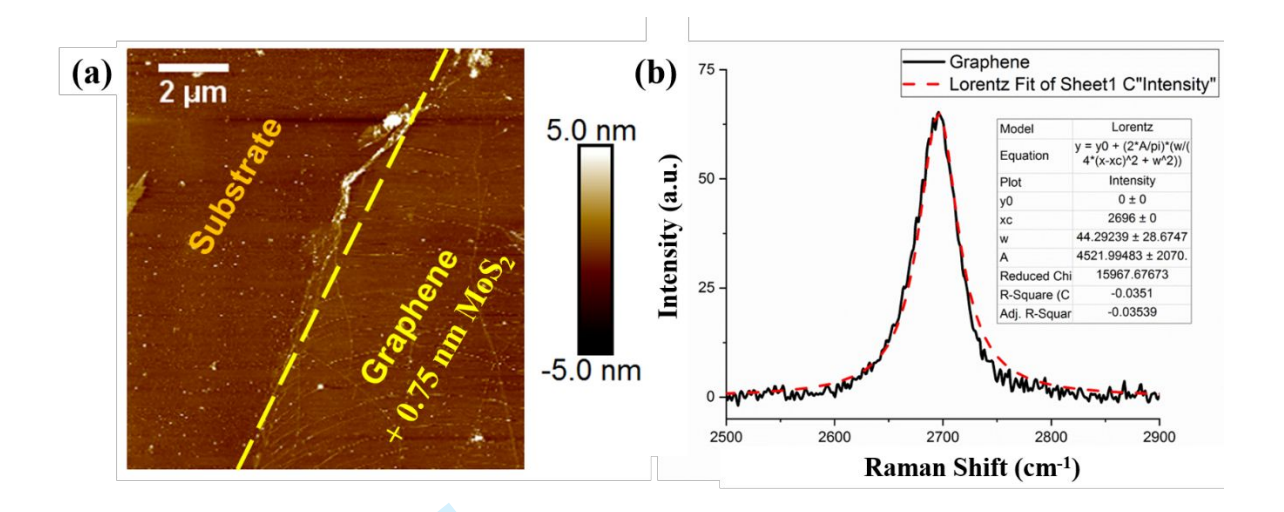


**Figure S2**. (a) AFM height image of a graphene layer atop a Si substrate. For this measurement, a 0.75 nm thick  $MoS_2$  layer was sandwiched between graphene and the substrate. At the edge of the graphene layer, there is a total step height increase of 1 nm, indicating that the thickness of the graphene layer was 0.25 nm. (b) Zoomed-in micro-Raman spectrum for the graphene layer showing 2D band. The original curve (black) can be represented by a single Lorentzian fit (red), which indicates the existence of single-layered graphene. If multiple layers exist, the 2D band can instead be divided into multiple fits, eventually splitting into two Gaussian peaks for graphite.

Policy.

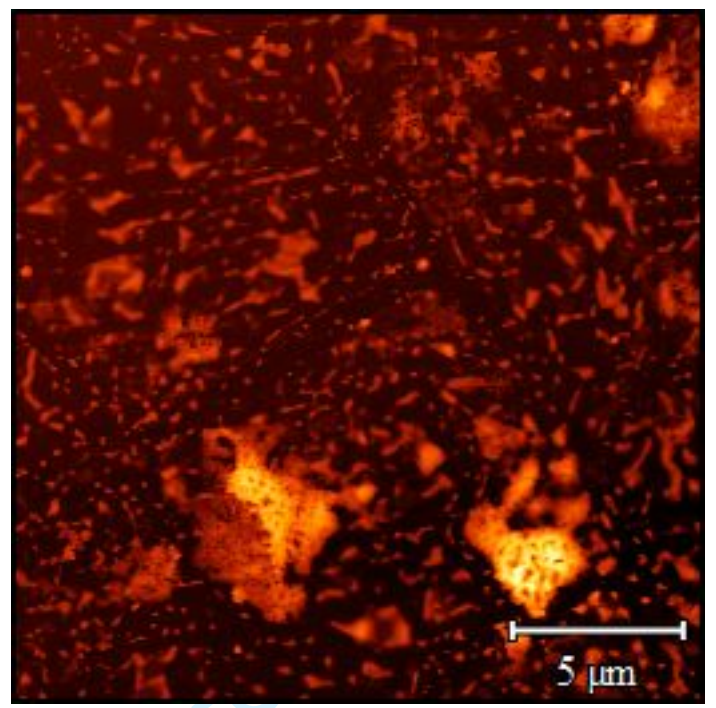


**Figure S3**. AFM height image of MAPLE-deposited PE crystals atop graphene. The substrate temperature was held constant at 100  $^{\circ}$ C during the deposition. The scale bar marks the length of 5  $\mu$ m.

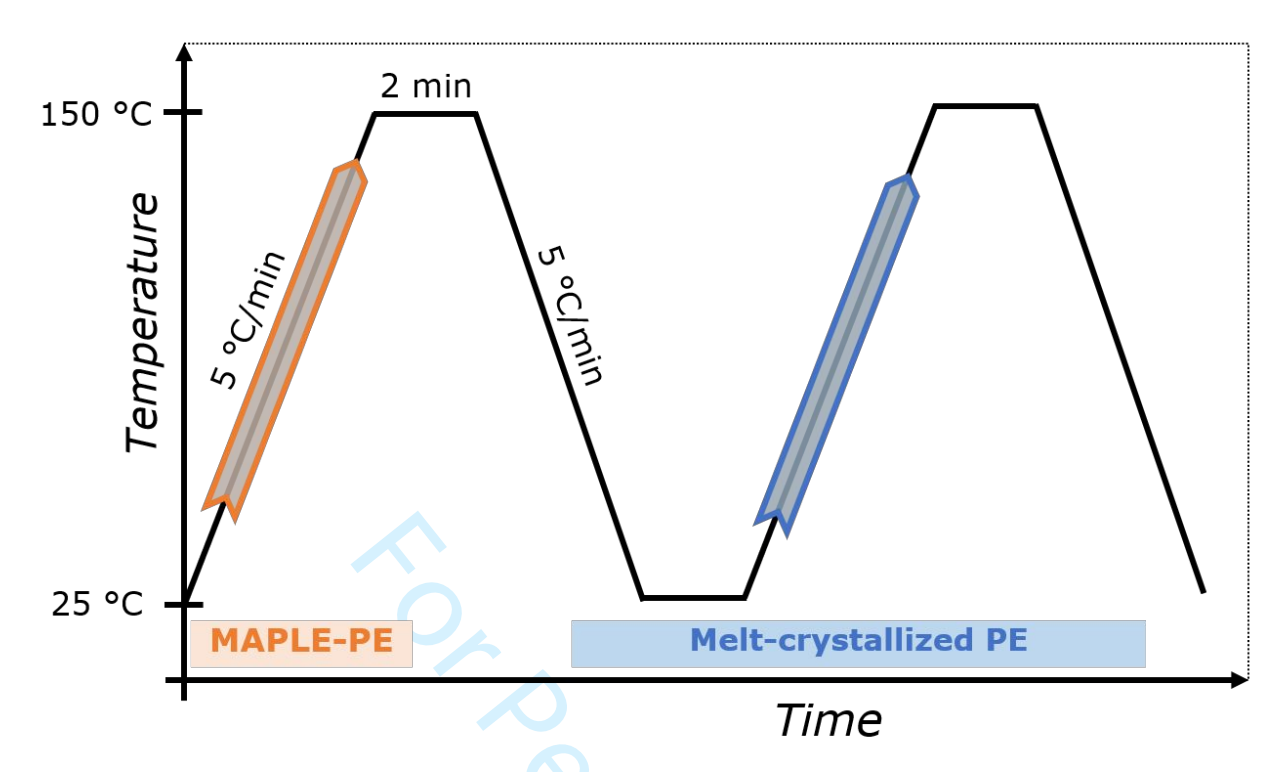


**Figure S4**. The thermal cycling protocol for in-situ GIXD measurements to investigate  $T_m$  and  $T_c$  of PE crystals atop the graphene surface. Two identical cycles were used to compare MAPLE-deposited PE and melt-recrystallized PE.

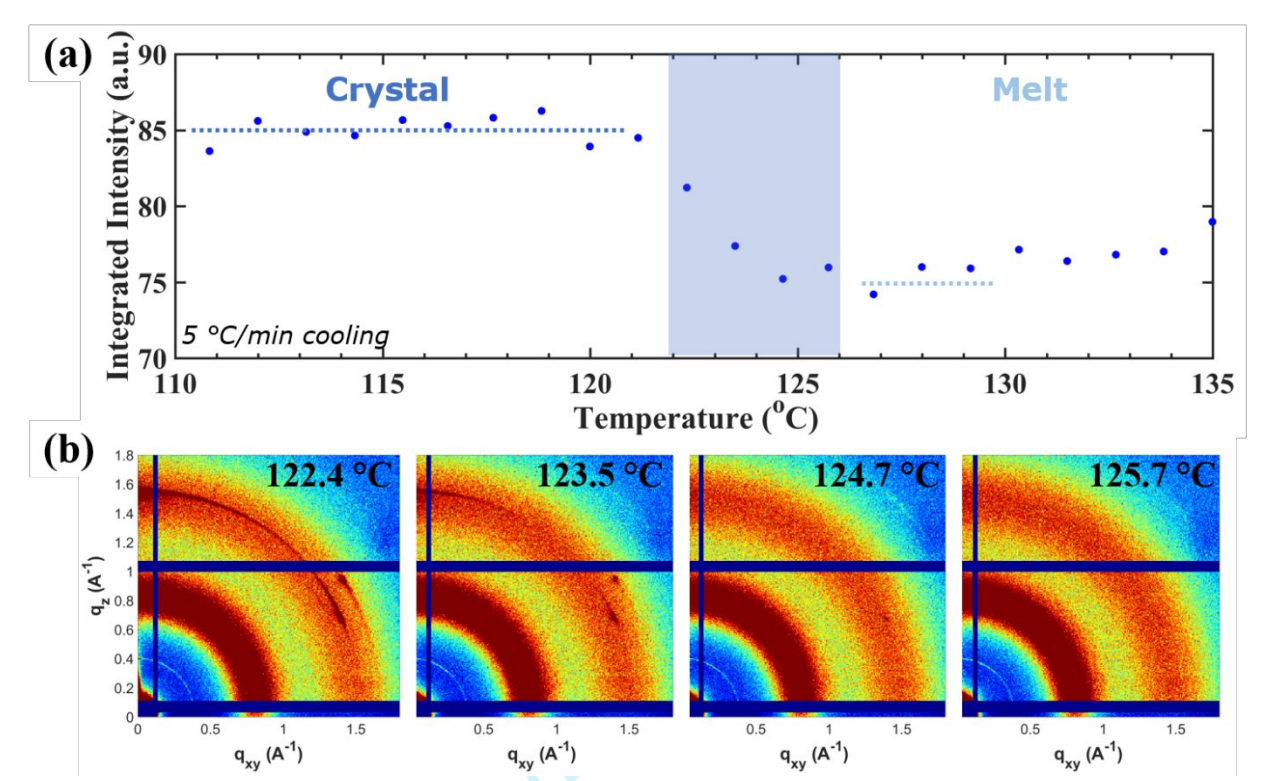
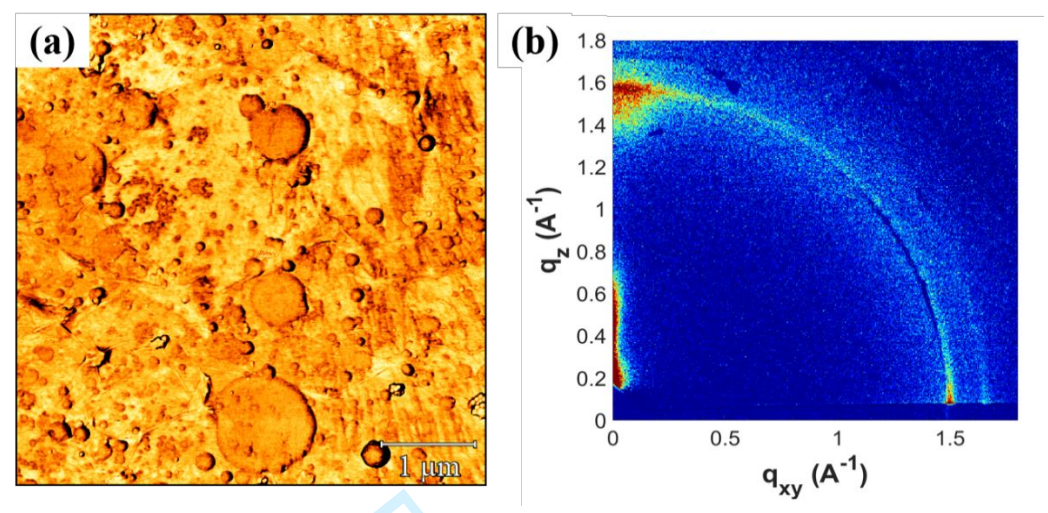


Figure S5. GIXD results measuring  $T_c$  of epitaxial crystallization of PE atop graphene from the melt. (a) Plot showing integrated intensity of PE crystal reflections as a function of temperature. The cooling rate was 5 °C/min. (b) The corresponding snapshots of GIXD in the vicinity of crystallization.



**Figure S6**. (a) AFM phase image of MAPLE-deposited PE crystals atop graphene. The substrate temperature was held constant at 25 °C during the deposition. The scale bar is 1  $\mu$ m. Compared to the morphology resulting at  $T_{sub}$  = 100 °C, PE crystals are much less oriented and are composed of nanoglobular shaped crystal domains. (b) The corresponding GIXD pattern collected at room temperature.